Method to derive ocean absorption coefficients from remote-sensing reflectance

Z. P. Lee, K. L. Carder, T. G. Peacock, C. O. Davis, and J. L. Mueller

A method to derive in-water absorption coefficients from total remote-sensing reflectance (ratio of the upwelling radiance to the downwelling irradiance above the surface) analytically is presented. For measurements made in the Gulf of Mexico and Monterey Bay, with concentrations of chlorophyll-a ranging from 0.07 to 50 mg/m^3, comparisons are made for the total absorption coefficients derived with the suggested method and those derived with diffuse attenuation coefficients. For these coastal to open-ocean waters, including regions of upwelling and the Loop Current, the results are as follows: at 440 nm the difference between the two methods is 13.0% ($r^2 = 0.96$) for total absorption coefficients ranging from 0.02 to 2.0 m^{-1}; at 488 nm the difference is 14.5% ($r^2 = 0.97$); and at 550 nm the difference is 13.6% ($r^2 = 0.96$). The results indicate that the method presented works very well for retrieval of in-water absorption coefficients exclusively from remotely measured signals, and that this method has a wide range of potential applications in oceanic remote sensing.

Key words: Remote-sensing reflectance, simulation of pigment absorption coefficients, diffuse attenuation coefficients.

1. Introduction

An important application of remote sensing is to quantify in-water inherent optical properties, which in turn can be used to estimate biomass,[1] primary production,[2] and heat flux.[3] The most important of the inherent optical properties is the absorption coefficient, as it dominates the downwelling attenuation coefficient and plays an essential role in energy transfer (e.g., primary production or heat). Empirical and semianalytical approaches for the derivation of the diffuse attenuation coefficient based on in-water or remote measurements have been discussed.[4,5] We suggest a method to derive analytically the absorption spectrum of ocean waters exclusively from remote-sensing measurements, and validation comparisons are made with values derived from in-water measurements.

The method suggested uses remote-sensing reflectance, the ratio of output radiance to input total irradiance. In ocean optics, input total irradiance is the downwelling irradiance above the surface (E_d; symbols used in this paper are summarized in Table 1), and output radiance is the radiance emanating from the sea surface. Traditionally, water remote-sensing reflectance (R_{rs}), which is the ratio of the water-leaving radiance (L_w) to E_d, has been used for applications such as the derivation of in-water pigment concentration.[6] Because of reflection of skylight from the sea surface, however, it is not always easy to measure R_{rs} accurately, as the sea surface is not flat. In this paper, instead of using R_{rs}, we use total remote-sensing reflectance (T_{rs}), which is defined as the ratio of upwelling radiance above the surface (L_u) to E_d. The absorption coefficient spectrum of the ocean is then derived from T_{rs}.

2. Theoretical Considerations

Upwelling radiance above the surface can be expressed as[7]

$$L_u = L_w + rL_{sky} + \Delta E_d, \quad (1)$$

where L_{sky} is the sky radiance that is reflected into the sensor by the water surface, r is the Fresnel reflectance of the interface, Δ is a spectral constant, and ΔE_d accounts for possible Sun glint and reflected cloud light from the uneven sea surface.[8] Note that wavelength dependency has been suppressed for brevity.

Z. P. Lee, K. L. Carder, and T. G. Peacock are with the Department of Marine Science, University of South Florida, 140 7th Avenue South, St. Petersburg, Florida 33701. C. O. Davis is with the Naval Research Laboratory, Washington, D.C. 20375. J. L. Mueller is with the Center of Hydro-Optics and Remote Sensing, San Diego State University, San Diego, California 92120.

Received 15 May 1995; revised manuscript received 21 August 1995.

0003-6935/96/030453-10$06.00/0

Table 1. List of Symbols

Symbol	Units	Description	Symbol	Units	Description
a	m^{-1}	total absorption coefficient, $a_w + a_g + a_p$	L_{sky}	W m^{-2} sr^{-1}	sky radiance that enters a remote sensor by the surface reflectance
a_{dg}	m^{-1}	absorption coefficient of the sum of detritus and gelbstoff	L_w	W m^{-2} sr^{-1}	water-leaving radiance
$a_{d,g,p,w,ph}$	m^{-1}	absorption coefficients of detritus, gelbstoff, particles, water, and pigments, respectively	n	—	refractive index of sea water
			R_G	—	reflectance of a diffuse reflector
			R_{rs}	sr^{-1}	water remote-sensing reflectance (L_w/E_d)
apd	—	average percentage difference, used to quantify the difference between the measured and modeled T_{rs}	$\overline{R}_{rs}$	sr^{-1}	measured R_{rs}
			$\check{R}_{rs}$	sr^{-1}	modeled R_{rs}
$a_{ph1,ph2}$	m^{-1}	absorption coefficients of pigments at the blue and the red peaks, respectively	S_{rs}	sr^{-1}	sky input (L_{sky}/E_d)
			$\overline{S}_{rs}$	sr^{-1}	measured S_{rs}
			T_{rs}	sr^{-1}	total remote-sensing reflectance (L_u/E_d)
AVG	—	average	$\overline{T}_{rs}$	sr^{-1}	measured T_{rs}
b_b	m^{-1}	backscattering coefficient	$\check{T}_{rs}$	sr^{-1}	modeled T_{rs}
$b_{bw,bp}$	m^{-1}	backscattering coefficients of water and particles, respectively	t	—	air–sea interface transmittance
			X	m^{-1} sr^{-1}	parameter to describe particle scattering
Chl	mg m^{-3}	chlorophyll-a concentration			
E_d	W m^{-2}	downwelling irradiance			
$\overline{E}_d$	W m^{-2}	measured E_d	Y	—	wavelength power to describe particle scattering
F	—	parameter to express a_{ph}			
g	—	constant to relate R_{rs} and b_b/a	Δ	sr^{-1}	offset of Sun glint because of waves or foam
I	—	divergence factor for radiance across the air–sea interface	ϵ	—	difference (error) between measured and calculated values
j	rad	subsurface solar-zenith angle			
K_d	m^{-1}	diffuse attenuation coefficient of downwelling irradiance	φ	rad	azimuth angle
			$\mu_d(0)$	—	subsurface average cosine for downwelling light field
$K_{d,av}$	m^{-1}	vertical average of K_d in the euphotic zone	μ_d	—	$f\mu_d(0)$, effective average cosine for downwelling light field
L	W m^{-2} sr^{-1}	radiance	λ	nm	wavelength
L_G	W m^{-2} sr^{-1}	radiance from diffuse reflector	η	—	wavelength power of particle backscattering coefficient
L_u	W m^{-2} sr^{-1}	upwelling radiance above the surface	Θ	rad	zenith angle

Dividing both sides of Eq. (1) by E_d provides

$$T_{rs} = R_{rs} + rS_{rs} + \Delta, \tag{2}$$

where R_{rs} is the water remote-sensing reflectance and S_{rs} is the sky input, defined respectively as

$$R_{rs} = \frac{L_w}{E_d}, \tag{3}$$

$$S_{rs} = \frac{L_{sky}}{E_d}. \tag{4}$$

In Eq. (2), both T_{rs} and S_{rs} can be easily measured, but only R_{rs} contains information regarding the in-water constituents.

Through Monte Carlo simulations for optically deep water, Gordon *et al.*[9] found that for nadir-view R_{rs} and a calm sea surface,

$$\check{R}_{rs} \approx \sum_{i=1}^{2} g_i \left(\frac{b_b}{a + b_b}\right)^i, \tag{5}$$

with $g_1 \approx 0.0949I$ and $g_2 \approx 0.0794I$. Here $\check{R}_{rs}$ stands for modeled R_{rs}, and $I \approx t^2/n^2$ is the air–sea interface divergence factor[7] (t is the air–sea transmittance, n is the refractive index of sea water).

The total backscattering coefficient $b_b = b_{bw} + b_{bp}$, where $b_{bw}(\lambda) = 0.0038(400/\lambda)^{4.3}$ is the backscattering coefficient for water molecules[10,11] and b_{bp} is the backscattering coefficient for suspended particles. $b_{bp}(\lambda)$ can be expressed as[11,12]

$$b_{bp}(\lambda) = b_{bp}(400)\left(\frac{400}{\lambda}\right)^{\eta}. \tag{6}$$

The total absorption coefficient $a = a_w + a_g + a_p$, in which a_w is the absorption coefficient for sea–water molecules and is given by Smith and Baker,[11] a_p is the absorption coefficient for suspended particles, and a_g is the absorption coefficient for gelbstoff (yellow substance, or colored dissolved organic matter). a can also be expressed as[6,13] $a = a_w + a_g + a_d + a_{ph}$, with a_{ph} for the absorption coefficient of phytoplankton pigments and a_d for the absorption coefficient of detritus. $a_g + a_d$ can be expressed as[6,13]

$$a_{dg} = a_{dg}(440)\exp[-S_{dg}(\lambda - 440)]. \tag{7}$$

Recently, Morel and Gentili[14] found through Monte

Carlo simulations that R_{rs} for sensors in a remote-sensing configuration[14] can be approximated as

$$\check{R}_{rs} \approx g\,\frac{b_b}{a}, \tag{8}$$

with $g \approx 0.0936I$ for λ from 440 to 550 nm. The value 0.0936 varies slightly with wavelength and light-field geometry.[14]

Through single and quasi-single-scattering theory,[15,16] Lee *et al.*[17–19] found that measured deep-water R_{rs} can be well modeled as

$$\check{R}_{rs} \approx \frac{G}{a}\left[\frac{b_{bw}}{3.4} + X\left(\frac{400}{\lambda}\right)^{Y}\right], \tag{9}$$

where $G \approx 0.32\,I$ (Ref. 20) and X and Y are spectral constants.

For cases in which $b_b \ll a$, approximations (5), (8), and (9) have almost the same denominator but different expressions for the numerator. If we express $b_b(\lambda)$ as $b_{bw}(\lambda) + X'(400/\lambda)^{Y'}$, then $Y' \approx Y$ and $X' \approx 3.42X + 0.0055b_{bw}(400)$. This means that mathematically approximation (8) and (9) are essentially equivalent, as $0.0055b_{bw}(400)$ is very small relative to $3.42X$. Optically, approximation (8) emphasizes that R_{rs} is characterized by the ratio of the backscattering coefficient to the absorption coefficient, and approximation (9) emphasizes that R_{rs} is characterized by the ratio of volume-scattering-function effects to the absorption coefficient.[19] As approximations (5), (8), and (9) are mathematically equivalent, and approximation (9) was developed based on field measurements, approximation (9) will be used in the following study.

Replacing R_{rs} in Eq. (2) with approximation (9), we can model T_{rs}

$$\check{T}_{rs} \approx \frac{G}{a}\left[\frac{b_{bw}}{3.4} + X\left(\frac{400}{\lambda}\right)^{Y}\right] + rS_{rs} + \Delta. \tag{10}$$

Now, let us assume that $\check{T}_{rs} = \overline{T}_{rs}$ (the measured values); then the ultimate question is how to retrieve useful in-water information from $\overline{T}_{rs}$.

For $\overline{T}_{rs}$ spectra from deep waters at N wavelengths $(\lambda_1, \lambda_2, \ldots, \lambda_N)$, ignoring gelbstoff fluorescence and water Raman scattering,[18,19,21,22] there are N equations:

$$\begin{aligned}
\overline{T}_{rs}(\lambda_1) &\approx \frac{0.17}{a_w(\lambda_1) + a_{dg}(\lambda_1) + a_{ph}(\lambda_1)} \\
&\quad \times \left[\frac{b_{bw}(\lambda_1)}{3.4} + X\left(\frac{400}{\lambda_1}\right)^{Y}\right] + rS_{rs}(\lambda_1) + \Delta, \\
&\vdots \\
\overline{T}_{rs}(\lambda_N) &\approx \frac{0.17}{a_w(\lambda_N) + a_{dg}(\lambda_N) + a_{ph}(\lambda_N)} \\
&\quad \times \left[\frac{b_{bw}(\lambda_N)}{3.4} + X\left(\frac{400}{\lambda_N}\right)^{Y}\right] + rS_{rs}(\lambda_N) + \Delta,
\end{aligned} \tag{11}$$

where 0.17 derives from $0.32I = 0.32\,(0.98/134)^2 \approx 0.17$.

In the N equations, $S_{rs}(\lambda)$ can be tightly modeled with three parameters if there are no sky radiance measurements. If there are sky radiance measurements, the number of parameters can be reduced to 2. To simplify the case, let us assume that S_{rs} can be replaced by the measured values $\overline{S}_{rs}$; then the number of unknowns for the N equations is $N + 6$, i.e., N for $a_{ph}(\lambda)$, 2 for $a_{dg}(\lambda)$ [$a_{dg}(440)$ and S_{dg}], 2 for particle scattering (X and Y), and 2 for r and Δ. If only $\overline{T}_{rs}$ is available, there will be no certain solution for the above equations unless we dramatically reduce the unknowns regarding $a_{ph}(\lambda)$.

3. Simulation of $a_{ph}(\lambda)$

Bidigare *et al.*[23] pointed out that a_{ph} can be reconstructed if the concentrations and the specific absorption coefficients for each pigment are known, but these cannot be known based only on remotely sensed data. Hoepffner and Sathyendranath[24] suggested that a_{ph} can be modeled by a sum of 11 Gaussian bands. The center wavelengths and half-bandwidths of these 11 bands would vary from phytoplankton species to species. Even if the center wavelengths and half-bandwidths can be determined, we still need 11 parameters to simulate $a_{ph}(\lambda)$, which would be too many for the available channels on some satellite sensors, such as the Coastal Zone Color Scanner and the Sea-Viewing Wide Field-of-View Sensor.

Methods that use the specific absorption coefficient spectrum[25] or the averaged absorption coefficient curves[26] for subsurface irradiance reflectance have also been suggested. With these approaches, only one unknown (the pigment concentration or a scale factor) is needed to model $a_{ph}(\lambda)$. Thus, if N is ≥ 7, theoretically the series of N equations could be solved and the unknowns related to the absorption, and scattering could be derived. However, these methods require prior knowledge of the a_{ph} curvature for every region[26] and its variation with season. Also, because of the package effect and changing light environments, it is well known that the a_{ph} curves vary widely from sample to sample.[23–27] No single shape for a_{ph} can be used for any water environments at any time. So for the inverse problem in remote sensing, which is to derive in-water information from remotely sensed data alone, simpler expressions with adequate accuracy for $a_{ph}(\lambda)$ would be very useful. Section 3 introduces a simple method to simulate $a_{ph}(\lambda)$ that takes the change of $a_{ph}(\lambda)$ shape into consideration.

Analysis of a_{ph} data collected from the Gulf of Mexico in April 1993 (28 samples), which covered a chlorophyll concentration range from 0.1 to 40 mg/m^3, led to a suggested expression for $a_{ph}(\lambda)$ by Lee.[19] This expression is a combination of three simple functions involving six parameters. Among the six

parameters, two parameters vary only slightly for different waters, and only two parameters have strong effects on the entire $a_{ph}(\lambda)$ curve. For the wavelength range of 400 nm $\le \lambda \le$ 700 nm, this simple mathematical simulation for $a_{ph}(\lambda)$ is

$$a_{ph}(\lambda) = a_{ph1} \exp\left[-F\left(\ln \frac{\lambda - \lambda_1}{100}\right)^2\right], \quad 400 \le \lambda \le 570, \tag{12a}$$

$$a_{ph}(\lambda) = a_{ph}(570) + \frac{a_{ph}(656) - a_{ph}(570)}{656 - 570}(\lambda - 570), \quad 570 < \lambda < 656, \tag{12b}$$

$$a_{ph}(\lambda) = a_{ph2} \exp\left[-\frac{(\lambda - \lambda_2)^2}{2\sigma^2}\right], \quad 656 \le \lambda \le 700. \tag{12c}$$

Figure 1 shows examples of measured versus simulated $a_{ph}(\lambda)$ curves, which are normalized at 440 nm. For the 28 samples used in the $a_{ph}(\lambda)$ simulation study, the average difference is 11% if the samples are compared wavelength by wavelength.[19] However, the difference drops to approximately 2% when we compare the integrated $a_{ph}(\lambda)$ values from 400 to 700 nm.

In Eqs. (12), there are six parameters: a_{ph1}, F, λ_1, a_{ph2}, λ_2, and σ. Parameter F describes the width of the a_{ph} curve from 400 to 570 nm, $(100 + \lambda_1)$ is the wavelength of the blue peak, λ_2 is the wavelength of the red peak, and 2.355σ determines the half-bandwidth around the red peak. For the samples in the report,[19] F varied from 1.6 to 4.2; λ_1 varied from 338 to 342 nm, with 80% of the values being equal to 340 nm; λ_2 varied from 672 to 675 nm, with most values at 674 nm; and 2.355σ ranged from 21 to 34 nm. a_{ph1} varied from 0.01 to 0.83 m^{-1}, and a_{ph2}/a_{ph1} varied from 0.21 to 0.85. Among the six parameters, λ_1 and λ_2 did not vary significantly, and a_{ph2} and σ only affect a small range of the a_{ph} curves, where the total absorption coefficients are dominated by the absorption of water molecules. Thus, only two parameters, a_{ph1} and F, are very important to the a_{ph} curve at wavelengths where significant light is absorbed by phytoplankton.

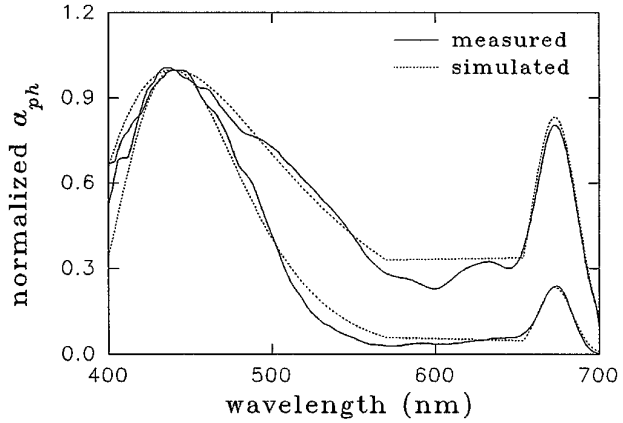

Fig. 1. Examples of $a_{ph}(\lambda)$ simulation (normalized at 440 nm, adapted from Lee[19]).

F, σ, and a_{ph2}/a_{ph1} are indicators of the package effect. The greater the package effect, the smaller the parameter F, the bigger the bandwidth 2.355σ, and the larger the ratio a_{ph2}/a_{ph1}. This means that for in vitro phytoplankton pigment absorption coefficients (i.e., no package effect), the fatness factor F will be close to 4.2, a_{ph2}/a_{ph1} is around 0.2, and the half-bandwidth (2.355σ) around the red peak will be close to 21 nm (a value similar to that reported by Hoepffner and Sathyendranath[24]).

The a_{ph} simulation parameters can be related to a_{ph1} after nonlinear regression analysis.[19] It was found that

$$a_{ph2}/a_{ph1} = 0.86 + 0.16 \ln(a_{ph1}), \quad \text{normalized rms error } 17.2\%,$$
$$F = 2.89 \exp[-0.505 \tanh[0.56 \ln(a_{ph1}/0.043)]], \quad \text{normalized rms error } 12.4\%,$$
$$\sigma = 14.17 + 0.9 \ln(a_{ph1}), \quad \text{normalized rms error } 5.6\%.$$

So, whenever we have a value for a_{ph1}, we can have a simulated $a_{ph}(\lambda)$ spectrum based on the relation above. However, for different a_{ph1} values, the shapes of the $a_{ph}(\lambda)$ spectra will also be different, as the package effect is taken into account, at least to the first order.

4. Absorption-Coefficient Retrieval from $\overline{T}_{rs}$

From the above a_{ph} simulations, if we fix λ_1 and λ_2 at 340 nm and 674 nm, respectively, and use the relation for a_{ph2}/a_{ph1}, F, and σ versus a_{ph1}, the number of total unknowns for the N equations is reduced to seven: a_{ph1}, $a_{dg}(440)$, S_{dg}, X, Y, r, and Δ. Now it is possible to derive the seven unknowns if $N \ge 7$.

In our hyperspectral field measurements, there are approximately 200 spectral channels for each $\overline{T}_{rs}$ and $\overline{S}_{rs}$ measurement, or approximately 200 equations. To minimize random error in the measurements (e.g., CCD readout noise), we used all the available channels.

We have used a goodness-of-fit parameter called average percentage difference (apd), defined as

$$apd = \frac{[\mathrm{AVG}_{400}^{660}(R_{rs} - \check{R}_{rs})^2 + \mathrm{AVG}_{750}^{830}(R_{rs} - \check{R}_{rs})^2]^{0.5}}{\mathrm{AVG}_{400}^{660}(R_{rs}) + \mathrm{AVG}_{750}^{830}(R_{rs})}. \tag{12}$$

$\mathrm{AVG}_{\lambda 1}^{\lambda 2}$ is the average value in the wavelength range λ_1 to λ_2. The cutoff between 660 and 750 nm is due to the fact that no term is included in the model to express the solar-stimulated chlorophyll fluorescence present in the measured data. The 750-to-830-nm band is important for turbid water environments.

By minimizing *apd*, one can derive a set of parameters, a_{ph1}, $a_{dg}(440)$, X, and Y. Before we do this, however, ranges for the unknowns have to be set because there exist realistic limits for them. It is possible that mathematical values outside of these limits may provide smaller *apd* values.

For the exponent Y, there are no direct measurements available. Part of Y is η [see Eq. (6)], which changes with the particle suite and size. Generally, it is assumed that $\eta \sim 1.0$ for low-chlorophyll open-ocean regions, and that $\eta \sim 0$ for coastal waters,[5,28] although η can be as high as 3.0 for coccolithophorid blooms.[29] Because of the similar curvature shapes of the b_b and a_{dg} spectra, however, the range for Y cannot simply be set as $0 \le Y \le 3$. When the absorption is dominated by a_{dg} (very common for coastal waters), the compensation between the a_{dg} and b_b parameters becomes strong, and small amounts of noise or error can affect wide swings in the parameterization. Therefore a narrow range for Y for each station must be specified. From previous model results,[18] a rough relation has been empirically derived: $Y \approx 0.86 + 1.2 \ln(\chi)$, with $\chi = R_{rs}(440)/R_{rs}(490)$. Thus the range for Y is chosen as

$$0.9[0.86 + 1.2 \ln(\chi)] \le Y \le 1.1[0.86 + 1.2 \ln(\chi)].$$

This keeps Y within 10% of the regression value for a station but still allows it to vary within $0 \le Y \le 3$ in general.

To provide the first iteration value, the water remote-sensing reflectance ($\overline{R}_{rs}$) is set by Eq. (2):

$$\overline{R}_{rs} \approx \overline{T}_{rs} - 0.018\overline{S}_{rs} - \Delta, \tag{14}$$

with Δ derived by forcing $R_{rs}(750) = 0$ because of the large water absorption at 750 nm. The Fresnel reflectance r is initially set to 0.018 in approximation (14) when a vertical polarizer is used for a nadir-viewing angle of $\le 30°$. It is adjusted to 0.03 as an initial value when there is no vertical polarizer in front of the sensor.

S_{dg}, which depends on the relative abundance between detritus and gelbstoff, varies from sample to sample.[13] By considering a detritus-to-gelbstoff absorption ratio at 440 nm of less than 1.0, we set the range for S_{dg} as

$$0.012 \le S_{dg} \le 0.016,$$

as the spectral slope for a_g is usually found within 0.011 to 0.019 nm^{-1} for various ocean waters,[30,31] with an average[32] of approximately 0.014 nm^{-1}.

The ranges for a_{ph1}, $a_{dg}(440)$, X, and r are much broader:

$$a_{ph1}, a_{dg}(440), X, r > 0.$$

With the above constraints, by minimizing *apd*, we derive the seven unknowns for measured $\overline{T}_{rs}$ curves from the waters of Monterey Bay and the Gulf of Mexico.

5. Derivation of the Total Absorption Coefficient from In-Water Measurements

Based on Monte Carlo simulations, Gordon[33] and Kirk[34] established that

$$a + b_b \approx f\mu_d(0)K_{d,av}, \tag{15}$$

where $K_{d,av}$ is the average downwelling diffuse attenuation coefficient in the euphotic zone. $\mu_d(0)$ is the subsurface downwelling average cosine and is approximately $\cos(j)$ for clear-sky days,[33,34] with j as the subsurface solar-zenith angle. f is a factor to account for the possible changes of the average cosine with increasing depth. In general f is less than 1.0, and through Monte Carlo simulations, Gordon[33] found that f is approximately 0.93. Kirk[34] found that f is a complicated function of $\mu_d(0)$ and the optical properties of the water.

As $I \approx 0.535$ ($t \approx 0.98$, $n \approx 1.34$), $R_{rs} \approx 0.05 b_b/a$ from approximation (8). Thus, at least to first order,

$$a \approx \frac{f\mu_d(0)K_{d,av}}{1 + 19.97R_{rs}}. \tag{16}$$

Therefore $K_{d,av}$, R_{rs}, and $\mu_d(0)$ have to be estimated in order to derive a with approximation (16) if we assume that $f = 0.93$.

The process of deriving $K_{d,av}$ is similar to that given by Smith and Baker.[11] Briefly, for the euphotic zone,

$$\overline{E}_d(z) = E_d(0^-)\exp(-K_{d,av}\overline{z}), \tag{17}$$

$$\ln[\overline{E}_d(z)] = \ln[E_d(0^-)] - K_{d,av}\overline{z}. \tag{18}$$

There are only two unknowns [$E_d(0^-)$ and $K_{d,av}$] in Eq. (18). However, because of effects from wave focusing and ship shadow,[35] the measured $\overline{E}_d(z)$ and $\overline{z}$ include errors associated with the field, so we cannot simply use values from two depths to derive $K_{d,av}$ and $E_d(0^-)$. In order to reduce those influences, linear regression between $\ln[\overline{E}_d(z)]$ and $\overline{z}$ were performed for the surface layer. The regression results provide $K_{d,av}$.

$\overline{R}_{rs}$ is the first-iteration value derived with approximation (14). This process may not provide the correct R_{rs}, however. Because the largest $R_{rs}(\lambda)$ value is about 0.005 sr^{-1}, a 100% error in R_{rs} at this scale will only cause a 10% error in a from approximation (16). So, as a simple procedure, the R_{rs} value derived with approximation (14) is accurate enough for the application of approximation (16).

For clear-sky days and no wave and ship influences, $\mu_d(0) \approx \cos(j)$.[33] However, for field measurements, clear-sky days are not always available, and there is some influence due to the ship presence.[35] Thus it is not easy to get the correct $\mu_d(0)$ for the variable field situations. In this case, to calculate a with approximation (16), we derived an effective μ_d [$= f\mu_d(0)$] for each station by forcing the $K_{d,av}$-derived $a(\lambda)$ to approximate $a_w(\lambda) + a_p(\lambda)$ for λ in the range of

600–660 nm. In this way, errors because of sea-surface roughness and ship presence could be reduced, and μ_d could be estimated for cloudy days when j was uncertain. Comparisons were made with results obtained when $f = 0.93$ and $\mu_d(0) = \cos(j)$ were used.

6. Field Measurements

A. $\overline{T}_{rs}$ and $\overline{S}_{rs}$

Using a Spectron Engineering spectroradiometer (Spectron Model SE-590), we measured hyperspectral $\overline{T}_{rs}$ and $\overline{S}_{rs}$ for sites in the Gulf of Mexico in April and June 1993 and for sites in Monterey Bay in September and October 1989. This covered coastal to open ocean waters, including regions of upwelling and the Loop Current. Both clear sky and variable cloudy sky situations were encountered. Briefly, the upwelling radiance above the surface $[\overline{L}_u(0^+, \Theta_a, \varphi)]$ was directly measured, with $\Theta_a \leq 30°$ from nadir and φ approximately 90° from the solar plane. Also directly measured was the downwelling sky radiance $(\overline{L}_{sky})$ in the same plane as $\overline{L}_u(0^+)$ but from a direction $\leq 30°$ from zenith. Downwelling irradiance was derived by measurement of the radiance $(\overline{L}_G)$ reflected from a standard diffuse reflector (Spectralon). Then downwelling irradiance is determined by

$$\overline{E}_d = \frac{\pi \overline{L}_G}{R_G}, \tag{19}$$

where R_G is the reflectance of the diffuse reflector ($\sim$10%).

B. $\overline{E}_d(z)$

Using a Biospherical Instruments Multichannel Environmental Radar (Model 1048A),[36] we measured the vertical profiles of the downwelling irradiance $[\overline{E}_d(z)]$ of the same sites as above.

7. Results and Discussion

For the above measurements, we derived a_{ph1}, $a_{dg}(440)$, X, and Y, as well as the total absorption coefficients $a(440)$, $a(488)$, and $a(550)$, from $\overline{T}_{rs}$ by minimizing *apd* for each station. Also, $K_{d,av}$ at 440, 488, and 550 nm and μ_d were derived for the same stations. The major results are summarized in Table 2. Figure 2 shows examples of $K_{d,av}$-derived a according to $a_w + a_p$, and Figs. 3 and 4 show measured $\overline{T}_{rs}$ and $\overline{S}_{rs}$. In the following, the $K_{d,av}$-derived a is considered as measured, and the $\overline{T}_{rs}$-derived a is considered as calculated.

Figure 5 compares the absorption coefficients derived from $\overline{T}_{rs}$ and K_d (by derived μ_d) at 440 nm. Figure 5(a) shows the values at each station, and Fig. 5(b) shows the values plotted against each other in a log–log format. Figures 6 and 7 compare the absorption coefficients derived from $\overline{T}_{rs}$ and K_d (by derived μ_d) at 488 nm and 550 nm, respectively.

Figure 8 shows examples of the derived and the simulated $R_{rs}(\lambda)$ curves, and Fig. 9 shows examples of the measured and the derived $a_{ph}(\lambda)$ curves. The derived $R_{rs}(\lambda)$ were from Eq. (2), with values for r and Δ from the minimizing process, and the simulated $R_{rs}(\lambda)$ were from approximation (9), with the derived a_{ph}, a_{dg}, X, and Y values. It can be seen that the $R_{rs}(\lambda)$ curves fit each other very well (with a 4% average *apd* for the 45 stations). The derived $a_{ph}(\lambda)$ also fit the measured $a_{ph}(\lambda)$ curves well.

We define the difference (error) between the values of the measured and the calculated curves, ϵ, as

$$\epsilon = \exp\left\{\text{AVG}\left[\left|\ln\left(\frac{\text{cal}}{\text{mea}}\right)\right|\right]\right\} - 1. \tag{20}$$

With a given ϵ, on average the measured value will fall in the range

$$\frac{\text{cal}}{1+\epsilon} \leq \text{mea} \leq (1+\epsilon)\text{cal}. \tag{21}$$

This method of error calculating emphasizes that equally large errors occur for underestimation and for overestimation. For example, errors are the same for cal/mea = 1/3 and for cal/mea = 3.0. However, traditional rms error is approximately 67% for cal/mea = 1/3 and 200% for cal/mea = 3.0.

From Eq. (20), the difference for $a(440)$ is 13.0% for $a(440)$ ranging from 0.02 to 2.0 m^{-1} (Chl ranged from 0.07 to 50 mg/m^3; see Table 2). Also, from Fig. 5, it can be seen that $\overline{T}_{rs}$-derived $a(440)$ is very consistent with the K_d-derived $a(440)$. By linear regression analysis, we find that r^2 is 0.96 ($n = 45$) between the two sets of results. Figures 6 and 7 compare $a(488)$ and $a(550)$ for the two methods. The correlation coefficient (r^2) for $a(488)$ is 0.97 between the two sets of results, with a 14.5% error, and r^2 for $a(550)$ is 0.96 with 13.6% error. These results suggested that the method to retrieve $a(\lambda)$ from $\overline{T}_{rs}(\lambda)$ works very well for this wide dynamic range of water types.

The 13.0% error for $a(440)$ can be caused by any of the following possible factors: (1) there may be errors in the $\overline{L}_u$, $\overline{L}_{sky}$, $\overline{E}_d(0^+)$, and $\overline{E}_d(z)$ measurements, which will be transferred to $\overline{T}_{rs}$, $\overline{S}_{rs}$, and $K_{d,av}$; (2) the model is developed for homogeneous water, whereas natural water is frequently patchy and somewhat stratified; (3) the a_{ph} simulation is not perfect; (4) there are inconsistencies between the $\overline{T}_{rs}$ and $\overline{E}_d(z)$ measurements as a result of patchiness; and (5) μ_d may be a function of wavelength.[33,34] With the consideration of these possible sources of error, a 13.0% error appears to be quite small, and it can be claimed that the method suggested can not only qualitatively but also quite accurately derive the in-water absorption coefficient for waters from coastal to open ocean.

It must be pointed out that the accuracy in deriving the individual components of the absorption coefficient is likely to be less than the accuracy in deriving the total absorption coefficient. A remote sensor gives one a measure of the total absorption, and the sensitivity of the sensor to an individual

Table 2. Summary of the Major Results

					Derived from K_d(av)			Derived from $\overline{T}_{rs}$								Derived from K_d(av)			Derived from $\overline{T}_{rs}$		
Station	Chl	K_d(440)	cos(j)	μ_d	a(440)	a(488)	a(550)	a(440)	a(488)	a(550)	Station	Chl	K_d(440)	cos(j)	μ_d	a(440)	a(488)	a(550)	a(440)	a(488)	a(550)
GO02[a]	21.00	1.487	0.96	0.62	0.850	0.852	0.580	1.102	0.654	0.369	CO01[b]	4.22	0.832	0.86	0.74	0.591	0.369	0.233	0.495	0.291	0.181
GO03	0.34	0.067	0.75	0.84	0.053	0.047	0.073	0.056	0.042	0.072	CO03	0.07	0.024	0.74	0.97	0.024	0.026	0.068	0.026	0.026	0.066
GO04	7.00	1.533	0.73	0.67	1.000	0.655	0.398	1.024	0.655	0.358	CO05	8.69	1.971	0.85	0.57	1.063	0.607	0.370	0.845	0.532	0.311
GO05	2.00	2.478	0.95	0.57	1.368	0.892	0.521	1.270	0.896	0.499	CO07	9.45	1.645	0.97	0.71	1.102	0.669	0.386	1.108	0.656	0.369
GO07	0.21	0.068	0.72	0.80	0.051	0.045	0.072	0.059	0.043	0.071	CO08	49.43	2.69	0.82	0.76	2.045	1.325	0.758	1.915	1.318	0.696
GO08	5.00	1.137	0.73	0.66	0.721	0.457	0.292	0.658	0.400	0.232	CO09	10.72	1.333	0.93	0.71	0.930	0.551	0.345	0.873	0.627	0.363
GO09	0.97	0.218	0.90	0.98	0.210	0.130	0.108	0.201	0.128	0.112	CO12	38.60	2.071	0.86	0.60	1.229	0.981	0.570	1.360	0.964	0.527
GO10	0.12	0.096	0.96	0.97	0.088	0.064	0.085	0.082	0.054	0.077	CO13	40.96	1.435	0.99	1.04	1.460	0.916	0.528	0.959	0.665	0.378
GO11	N/A	0.053	0.81	0.85	0.041	0.033	0.061	0.041	0.032	0.068	CO14	20.30	1.636	0.93	0.89	1.427	0.848	0.522	1.258	0.865	0.473
GO12	0.20	0.054	0.71	0.89	0.044	0.036	0.064	0.050	0.038	0.072	CO15	22.82	1.344	0.82	0.64	0.848	0.542	0.329	0.788	0.545	0.316
GO13	0.09	0.063	0.88	0.93	0.055	0.046	0.073	0.069	0.049	0.076	CO16	19.57	1.536	0.96	0.57	0.851	0.564	0.338	0.689	0.424	0.244
GO14	0.70	0.215	0.96	0.92	0.194	0.125	0.118	0.167	0.100	0.094	CO18	0.10	0.058	0.73	0.89	0.047	0.045	0.091	0.027	0.026	0.066
GO15	1.44	0.808	0.87	0.79	0.623	0.408	0.272	0.580	0.389	0.241	CO19	0.22	0.082	0.80	0.86	0.065	0.055	0.083	0.053	0.039	0.070
GO16	0.26	0.043	0.79	0.94	0.036	0.035	0.071	0.037	0.032	0.068	CO20	0.43	0.175	0.94	1.00	0.153	0.098	0.100	0.145	0.088	0.089
GO19	0.26	0.070	0.83	0.97	0.065	0.049	0.074	0.074	0.053	0.077	M9c5[c]	2.96	0.224	0.80	0.87	0.187	0.139	0.123	0.168	0.114	0.105
GO20	3.09	0.073	0.82	0.92	0.063	0.050	0.078	0.063	0.045	0.073	M9c7	2.30	0.239	0.90	0.84	0.193	0.150	0.126	0.176	0.117	0.103
GO22	0.42	0.272	0.75	0.75	0.180	0.125	0.121	0.141	0.090	0.095	M9c2	N/A	0.339	0.86	0.84	0.277	0.208	0.160	0.279	0.192	0.143
GO23	1.41	0.206	0.90	0.85	0.160	0.109	0.111	0.133	0.081	0.090	M9c3	N/A	0.305	0.90	0.86	0.250	0.185	0.146	0.242	0.170	0.132
GO24	0.30	0.123	0.97	0.98	0.112	0.078	0.085	0.107	0.065	0.080	M91c	N/A	0.333	0.89	0.89	0.287	0.219	0.160	0.306	0.217	0.156
GO25	0.23	0.089	0.80	0.89	0.075	0.054	0.079	0.074	0.052	0.077	M10c1[d]	3.68	0.696	0.68	0.63	0.415	0.342	0.243	0.427	0.297	0.193
GO26	0.30	0.186	0.69	0.77	0.134	0.092	0.099	0.112	0.074	0.087	M10m1	1.88	0.184	0.75	0.88	0.155	0.108	0.106	0.209	0.131	0.109
GO27	0.20	0.139	0.81	0.85	0.112	0.077	0.090	0.095	0.064	0.083	M10m4	1.29	0.239	0.84	0.76	0.171	0.132	0.121	0.163	0.111	0.103
GO28	0.18	0.078	0.95	0.99	0.072	0.055	0.081	0.079	0.052	0.077											

[a]GO, Gulf of Mexico, April 1993.
[b]CO, Gulf of Mexico, June 1993.
[c]M9, Monterey Bay, September 1989.
[d]M10, Monterey Bay, October 1989.

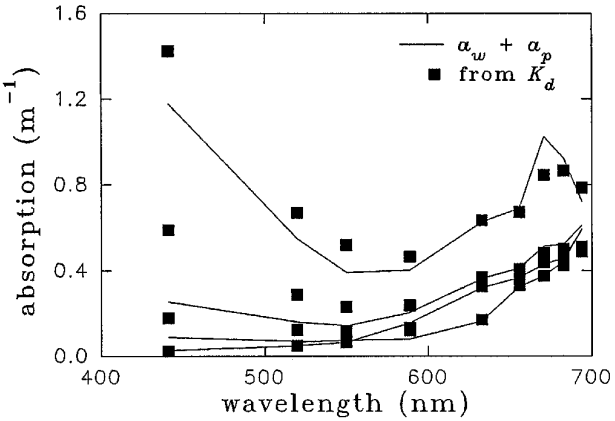

Fig. 2. Examples of $K_{d,\mathrm{av}}$-derived a based on $a_w + a_p$.

component of the absorption depends on the relative contribution of the individual component to the total and the uniqueness of its spectral shape relative to the other components in the total. If the contribution is small, the remote sensor may not be able to distinguish its change. However, if the contribution is large, the remote sensor may easily be able to observe the change. For the comparable data we have, the error is 37.9% when we compare derived and measured $a_{\mathrm{ph}}(440)$ values for the CO (June 1993,

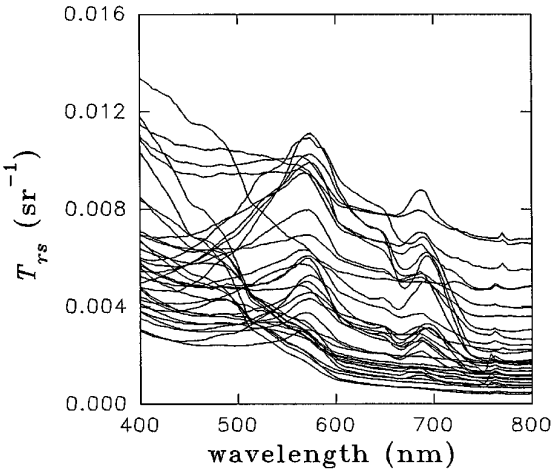

Fig. 3. Measured $\overline{T}_{\mathrm{rs}}$ of the stations.

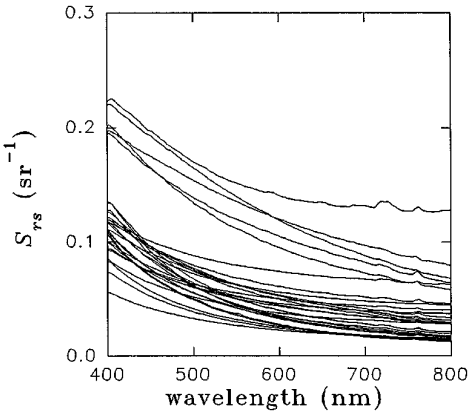

Fig. 4. Measured $\overline{S}_{\mathrm{rs}}$ of the stations.

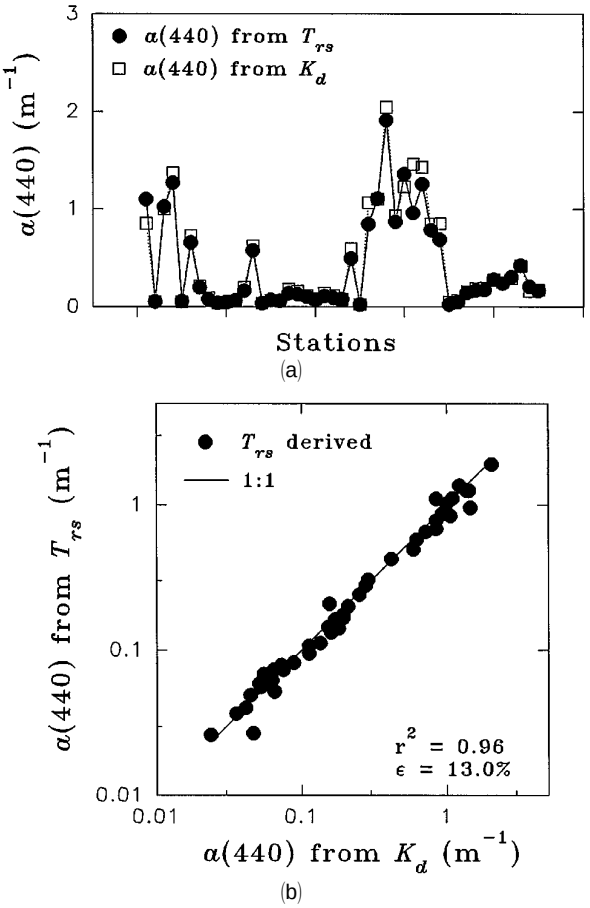

Fig. 5. (a) comparison of $a(440)$ following the cruise stations, (b) comparison of $a(440)$ values in a log–log plot.

Gulf of Mexico) cruise. It must also be pointed out that the derived $a_{\mathrm{ph}}(440)$ is an optical average of the upper water column, whereas measured $a_{\mathrm{ph}}(440)$ typically was derived from a sample collected at one depth. Also, the errors associated with the a_{ph} measurement were not determined.

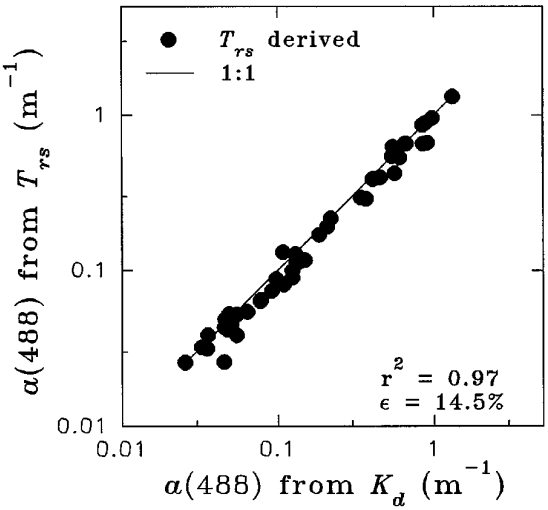

Fig. 6. Comparison of $a(488)$ values in log–log plot.

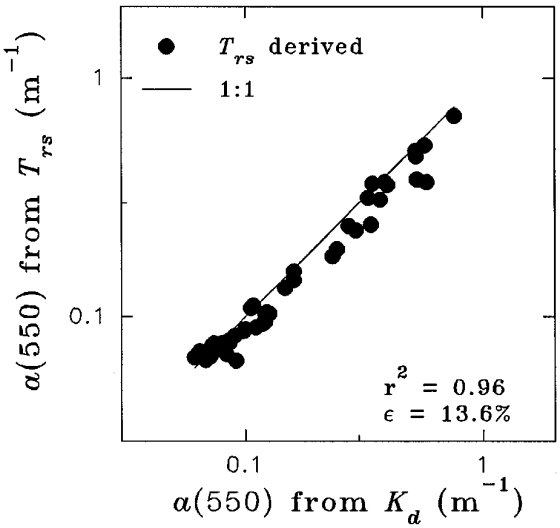

Fig. 7. Comparison of $a(550)$ values in log–log plot.

The $\cos(j)$ was calculated for each station assuming no influence from cloud, wave, and ship. When $\cos(j)$ was used to replace $\mu_d(0)$ in deriving a from $K_{d,\mathrm{av}}$, the error jumped to 25.9% for the same $a(440)$ range, with $r^2 = 0.93$. This suggests that the method used to derive μ_d is applicable and provides practical improvement over simply using $\cos(j)$.

It is interesting that the ratio of effective μ_d to $\cos(j)$ follows a relative trend against $K_d(440)$

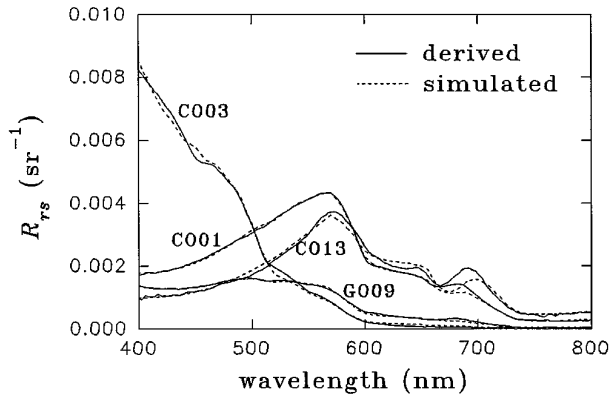

Fig. 8. Examples of derived and simulated $R_{\mathrm{rs}}(\lambda)$.

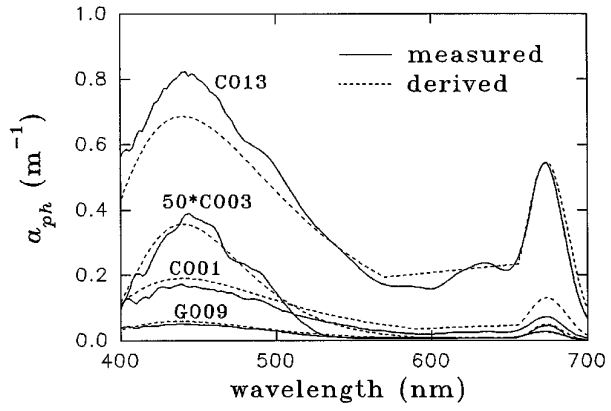

Fig. 9. Examples of derived and measured $a_{\mathrm{ph}}(\lambda)$.

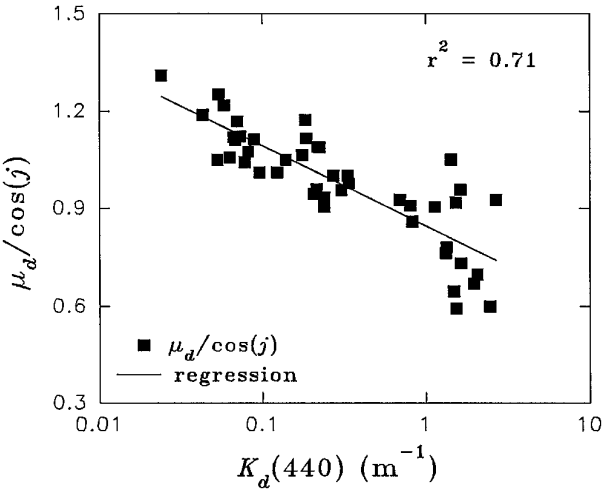

Fig. 10. $\mu_d/\cos(j)$ versus $K_d(440)$.

(Fig. 10). The regression result is

$$\frac{\mu_d}{\cos(j)} = 0.846 - 0.107 \ln[K_d(440)], \qquad (22)$$

with $r^2 = 0.71$. This is conceptually consistent with Kirk's Monte Carlo results,[34] as μ_d includes information about the radiance distribution in the upper layer and the $K_d(440)$ value provides an indicator of the water turbidity. Because in our data set μ_d was calculated for a variety of sky conditions, Eq. (22) provides a simple way to estimate the effective average cosine for the purpose of calculating a from K_d.

8. Conclusions

The simulation of $a_{\mathrm{ph}}(\lambda)$ works very well in the retrieval of the in-water absorption coefficients based exclusively on remotely measured data, at least for the data set reported here. Also, the ranges for the model parameters are consistent with ranges reported in the literature.

T_{rs}-derived total absorption coefficients are very consistent with the K_d-derived values, with only a 13.0% error for waters in which $a(440)$ ranged from 0.02 to 2.0 m^{-1} (Chl ranged from 0.07 to 50 mg/m^3).

Moreover, coupled in-water and remote-sensing measurements for a wide range of waters are needed in order to test and improve the suggested method, especially for the determination of the ranges of Y and S_{dg}, the retrieval of $a(\lambda)$ from $K_d(\lambda)$, and the simulation of $a_{\mathrm{ph}}(\lambda)$ when there are significant changes of phytoplankton species.

Financial support was provided by NASA through grant NAGW-465 and Goddard Space Flight Center contract NAS5-30779, and by the Office of Naval Research through grants N00014-89-J-1091 and N00014-95-I-0114. Ship support was provided by the R/V Suncoaster through the Florida Institute of Oceanography and the R/V Bartlett through the Navy Oceanography Office.

References

1. H. R. Gordon, R. C. Smith, and J. R. V. Zaneveld, "Introduction to ocean optics," in *Ocean Optics VI,* S. Q. Duntley, ed., Proc. Soc. Photo-Opt. Instrum. Eng. **208,** 1–43 (1980).
2. Z. P. Lee, K. L. Carder, J. Marra, R. G. Steward, and M. J. Perry, "Estimating primary production at depth from remote sensing," submitted to Appl. Opt.
3. M. R. Lewis, M. E. Carr, G. Feldman, C. McClain, and W. Esaias, "Influence of penetrating solar radiation on the heat budget of the equatorial Pacific ocean," Nature **347,** 543–545 (1990).
4. R. W. Austin and T. J. Petzold, "The determination of the diffuse attenuation coefficient of sea water using the Coastal Zone Color Scanner," in *Oceanography from Space,* J. F. R. Gower, ed. (Plenum, New York, 1981), pp. 239–256.
5. H. R. Gordon and A. Morel, *Remote Assessment of Ocean Color for Interpretation of Satellite Visible Imagery: A Review* (Springer-Verlag, New York, 1983), p. 35.
6. K. L. Carder, S. K. Hawes, K. A. Baker, R. C. Smith, R. G. Steward, and B. G. Mitchell, "Reflectance model for quantifying chlorophyll *a* in the presence of productivity degradation products," J. Geophys. Res. **96,** 20599–20611 (1991).
7. R. W. Austin, "Inherent spectral radiance signatures of the ocean surface," in *Ocean Color Analysis (Final Technical Report)*, S. Q. Duntley, ed., SIO Ref. 74-10 (Scripps Institution of Oceanography, La Jolla, Calif., 1974).
8. K. L. Carder and R. G. Steward, "A remote-sensing reflectance model of a red tide dinoflagellate off West Florida," Limnol. Oceanogr. **30,** 286–298 (1985).
9. H. R. Gordon, O. B. Brown, R. H. Evans, J. W. Brown, R. C. Smith, K. S. Baker, and D. K. Clark, "A semianalytic radiance model of ocean color," J. Geophys. Res. **93,** 10909–10924 (1988).
10. A. Morel, "Optical properties of pure water and pure sea water," in *Optical Aspects of Oceanography,* N. G. Jerlov and E. S. Nielsen, ed. (Academic, New York, 1974), pp. 1–24.
11. R. C. Smith and K. S. Baker, "Optical properties of the clearest natural waters," Appl. Opt. **20,** 177–184 (1992).
12. A. Morel and L. Prieur, "Analysis of variations in ocean color," Limnol. Oceanogr. **22,** 709–722 (1977).
13. C. S. Roesler, M. J. Perry, and K. L. Carder, "Modeling in situ phytoplankton absorption from total absorption spectra in productive inland marine waters," Limnol. Oceanogr. **34,** 1510–1523 (1989).
14. A. Morel and B. Gentili, "Diffuse reflectance of oceanic waters. II. Bidirectional aspects," Appl. Opt. **32,** 6864–6879 (1993).
15. H. R. Gordon, O. B. Brown, and M. M. Jacobs, "Computed relationship between the inherent and apparent optical properties of a flat homogeneous ocean," Appl. Opt. **14,** 417–427 (1975).
16. H. R. Gordon, "Modeling and simulating radiative transfer in the ocean," in *Ocean Optics,* R. W. Spinrad, K. L. Carder, and M. J. Perry, eds., Oxford Monographs on Geology and Geophysics 25 (Oxford University, New York, 1994), pp. 3–39.
17. Z. P. Lee, K. L. Carder, S. K. Hawes, R. G. Steward, T. G. Peacock, and C. O. Davis, "An interpretation of high spectral resolution remote sensing reflectance," in *Optics of the Air–Sea Interface,* L. Estep, ed., Proc. Soc. Photo-Opt. Instrum. Eng. **1749,** 49–64 (1992).
18. Z. P. Lee, K. L. Carder, S. K. Hawes, R. G. Steward, T. G. Peacock, and C. O. Davis, "A model for interpretation of hyperspectral remote sensing reflectance," Appl. Opt. **33,** 5721–5732 (1994).
19. Z. P. Lee, "Visible-infrared remote-sensing model and applications for ocean waters," Ph.D. dissertation (University of South Florida, St. Petersburg, Fla., 1994), Dissertation Abstract International 56-01B (UMI Microfilm, Ann Arbor, Mich., 1995).
20. J. H. Jerome, R. P. Bukata, and J. E. Burton, "Utilizing the components of vector irradiance to estimate the scalar irradiance in natural waters," Appl. Opt. **27,** 4012–4018 (1988).
21. D. Spitzer and R. W. J. Dirks, "Contamination of the reflectance of natural waters by solar-induced fluorescence of dissolved organic matter," Appl. Opt. **24,** 444–445 (1985).
22. B. R. Marshall and R. C. Smith, "Raman scattering and in-water ocean properties," Appl. Opt. **29,** 71–84 (1990).
23. R. R. Bidigare, M. E. Ondrusek, J. H. Morrow, and D. A. Kiefer, "In vivo absorption properties of algal pigments," in *Ocean Optics X,* R. W. Spinrad, ed., Proc. Soc. Photo-Opt. Instrum. Eng. **1302,** 290–302 (1990).
24. N. Hoepffner and S. Sathyendranath, "Effect of pigment composition on absorption properties of phytoplankton," Mar. Ecology Prog. Ser. **73,** 11–23 (1991).
25. A. Morel, "In-water and remote measurements of ocean color," Boundary-Layer Meteorol. **18,** 177–201 (1980).
26. C. S. Roesler and M. J. Perry, "In situ phytoplankton absorption, fluorescence emission, and particulate backscattering spectra determined from reflectance," J. Geophys. Res. **100,** 13279–13294 (1995).
27. A. Bricaud and D. Strasmski, "Spectral absorption coefficients of living phytoplankton and nonalgal biogenous matter: a comparison between the Peru upwelling area and the Sargasso Sea," Limnol. Oceanogr. **35,** 562–582 (1990).
28. A. Morel, "Optical modeling of the upper ocean in relation to its biogenous matter content (Case 1 waters)," J. Geophys. Res. **93,** 10749–10768 (1988).
29. H. R. Gordon, O. B. Brown, R. H. Evans, J. W. Brown, R. C. Smith, K. S. Baker, and D. K. Clark, "A semianalytic radiance model of ocean color," J. Geophys. Res. **93,** 10909–10924 (1988).
30. K. L. Carder, R. G. Steward, G. R. Harvey, and P. B. Ortner, "Marine humic and fulvic acids: their effects on remote sensing of ocean chlorophyll," Limnol. Oceanogr. **34,** 68–81 (1989).
31. S. K. Hawes, K. L. Carder, and G. R. Harvey, "Quantum fluorescence efficiencies of marine humic and fulvic acids: effects on ocean color and fluorometric detection," in *Ocean Optics XI,* G. D. Gilbert, ed., Proc. Soc. Photo-Opt. Instrum. Eng. **1750,** 212–223 (1992).
32. A. Bricaud, A. Morel, and L. Prieur, "Absorption by dissolved organic matter of the sea (yellow substance) in the UV and visible domains," Limnol. Oceanogr. **26,** 43–53 (1981).
33. H. R. Gordon, "Can the Lambert-Beer law be applied to the diffuse attenuation coefficient of ocean water?" Limnol. Oceanogr. **34,** 1389–1409 (1989).
34. J. T. O. Kirk, "Volume scattering function, average cosines, and the underwater light field," Limnol. Oceanogr. **36,** 455–467 (1991).
35. H. R. Gordon, "Ship perturbation of irradiance measurements at sea. 1: Monte Carlo simulations," Appl. Opt. **24,** 4172–4182 (1985).
36. J. L. Mueller and C. C. Trees, "Evaluation of coastal zone color scanner diffuse attenuation coefficient algorithms for application to coastal waters," in *Ocean Optics X,* R. W. Spinrad, ed., Proc. Soc. Photo-Opt. Instrum. Eng. **1302,** 72–78 (1990).